Clays and Clay Minerals, Vol. 56, No. 3, 344–358, 2008.

Na-BEARING WHITE MICAS FROM TRIASSIC ROCKS OF THE TRANSITION BETWEEN THE MALÁGUIDE AND ALPUJÁRRIDE COMPLEXES (BETIC CORDILLERA, SPAIN)

MARIA DOLORES RUIZ CRUZ*

Departamento de Química Inorgánica, Cristalografía y Mineralogía, Facultad de Ciencias, Universidad de Málaga, 29071 Málaga, Spain

Abstract—The structural significance of micas with Na-K intermediate composition, and their chemical and structural evolution at increasing metamorphic grade have been investigated in Triassic rocks from the transition between the Maláguide and Alpujárride complexes (Internal zones of the Betic Cordillera, Spain). Micas were studied by X-ray diffraction (XRD) and by scanning and transmission electron microscopy (SEM/TEM). Three samples, belonging to the late diagenesis and to the low and medium anchizone, were selected for this study. Na-bearing mica appears as submicroscopic packets intergrown in parallel with K-mica, becoming more compositionally uniform with increasing grade. The diagenetic sample contains illite, minor paragonite, and two main populations of intermediate Na-K micas, with average compositions $Ms_{60}Prg_{40}$ and $Ms_{35}Prg_{65}$, respectively, where Ms represents muscovite and Prg, paragonite. The lattice-fringe images of mica packets with intermediate compositions suggest the presence of random mixed-layered paragonite-muscovite. Under low anchizonal conditions the amount of discrete paragonite increases and the Na-K intermediate mica has a mean composition of $Ms_{40}Prg_{60}$. The TEM images suggest that the packets with intermediate composition are solid solutions of paragonite and illite. Micas with Na-K intermediate composition are lacking in the sample with the highest metamorphic grade. In this sample, paragonite and muscovite coexist with mica, with composition intermediate between paragonite and margarite. The lattice-fringe images of these Na-Ca-bearing packets suggest that they consist of irregularly shaped domains enriched either in Na or in Ca.

Our data indicate that Na+K-bearing micas have several origins: detrital stacks of K- and Na-bearing micas coexist with authigenic phases, formed from dickite in the diagenetic, coarse-grained samples, and perhaps from smectite-bearing mixed-layers or detrital illite, in the fine-grained rocks. The changes observed at increasing metamorphic grade can be related to the influence of the lithology, the metamorphic grade, and the different geological settings. Intermediate Na-Ca mica appears to have grown from paragonite, with calcite as the source of Ca.

Key Words—Intermediate Na-Ca mica, Intermediate Na-K mica, Low-grade Metamorphism, Muscovite, Paragonite.

INTRODUCTION

Micas having compositions intermediate between muscovite (or phengite) and paragonite have been identified many times in diagenetic-to-epizonal metapelites (Frey, 1987, and references therein) and in medium-grade metamorphic rocks (Guidotti, 1984; Shau *et al*., 1991). In most cases, intermediate compositions obtained from microprobe analyses are due to the presence of very fine-scale intergrowths of phengite and paragonite of nearly end-member composition (Ahn *et al.*, 1985; Ferrow *et al.*, 1990; Shau *et al.*, 1991; Boundy *et al.*, 1997; Martín-García *et al.*, 1997). Nevertheless, the existence of single-phase micas with compositions within the paragonite–muscovite solvus has also been proved based on XRD and TEM data (*e.g.* Jiang and Peacor, 1993).

These phases were first interpreted as mixed-layered paragonite/muscovite (*e.g.* Frey, 1969, 1970; Kisch, 1983; Merriman and Roberts, 1985), on the basis of the presence of a series of reflections at approximately fixed positions, intermediate between those of muscovite (10 Å) and paragonite (9.6 Å), and a small superstructure reflection, in the XRD patterns. Most recently, Na-K intermediate mica has been identified in hydrothermally altered rocks (Jiang and Peacor, 1993; Giorgetti *et al.*, 2003). These authors concluded, from detailed electron microscopic studies, that the compositionally intermediate mica was produced as a metastable phase during alteration. Li *et al.* (1992, 1994) described the presence of mica with intermediate Na-K composition in anchizonal mudrocks from central Wales. These authors deduced that bedding-parallel metastable mica with disordered distribution of K and Na formed from smectite during diagenesis. This intermediate mica evolved later to stable muscovite and paragonite, which follow the cleavage orientation. Livi *et al.* (1997) also showed an evolution from brammallite to paragonite in diagenetic to epizone-grade Liassic shales

* E-mail address of corresponding author:
mdruiz@uma.es
DOI: 10.1346/CCMN.2008.0560305

from the Alps. The Na-K-intermediate phases were interpreted as consisting of irregularly shaped Na- and K-rich domains.

Dioctahedral Na-K-mica and paragonite (or brammallite) are common constituents in Triassic sequences from the Internal zone of the Betic Cordillera. This zone is composed of three tectonically superimposed complexes which, from bottom to top, are: the Nevado-Filábride, the Alpujárride, and the Maláguide. In addition, transitional units with tectonic positions intermediate between the Alpujárride and the Maláguide complexes have been described in some areas of the cordillera (Sanz de Galdeano *et al.*, 2001). These units are ideal zones for studying the compositional and structural changes of the Na-bearing micas because the presence of numerous thinned thrust slices, some of which show metamorphic discontinuities at the boundaries, favors the identification of the mineral evolution in relatively restricted areas. The metamorphic grade ranges from the diagenetic zone in the upper slices to the epizone in the lower ones. Because the structural significance of micas with intermediate composition has been widely debated, and the intermediate units provide a very complete sequence of such white micas, the aim of this work is the study and interpretation of the chemical and structural evolution of these micas at increasing metamorphic grade, the analysis of their origin in the several lithologies, and the significance of this evolution in terms of 'metastable *vs*. stable structures'.

This study was based on the combination of XRD and SEM and TEM/analytical electron microscopy (AEM). The electron microscopy study is important for examining the textural relations among the several phases and to deduce the possible genetic relations between these. Nevertheless, the estimation of the relative amounts of the several micas and of their mean composition is notably easier from the XRD patterns.

GEOLOGICAL BACKGROND

The Triassic Maláguide units typically include red conglomerates, red sandstones, red lutites, and calcareous beds deposited in a continental environment (Mäkel, 1985). These sequences show diagenetic to low-anchizonal conditions of alteration (Ruiz Cruz and Rodríguez Jiménez, 2002). In contrast, typical Triassic sequences of the underlying Alpujárride complex include blue phyllites and schists, calcareous schists, minor sandstones, and marbles deposited in continental-to-shallow marine environments, *i.e.* more distal. These rocks contain evidence of a low-temperature/high-pressure metamorphism overprinted by a high-temperature/low-pressure one (Azañón *et al.*, 1997, 1998; Goffé *et al.*, 1989; Booth-Rea *et al.*, 2002). In the intermediate units, the uppermost thrust slices show lithological characteristics and metamorphic patterns similar to the those of the Maláguide complex, whereas at greater depth the units are characterized by the presence of intermediate lithologies and metamorphic patterns, passing into lithologies and mineral assemblages typical of the Alpujárride complex. Thus, a transition from sequences rich in coarse-grained rocks (sandstones and conglomerates), typical of the Maláguide complex, to primarily pelitic sequences, typical of the Alpujárride complex, characterizes the intermediate units.

The intermediate units were sampled at the Casares area (Figure 1), in the westernmost part of the Cordillera. In this area, four units were distinguished by Sanz de Galdeano *et al.* (1999), which from bottom to top are: Jubrique (clearly belonging to the Alpujárride complex), Rozalejo, Albarrán, and Rosales-Crestellina unit (the last of these with clear Maláguide affinity).

These units were sampled extensively and studied systematically by means of XRD and microprobe analysis (Ruiz Cruz *et al.*, 2006). This preliminary study revealed an evolution of the mineral assemblages. The upper slices show Al-rich assemblages consisting of illite + Na-K mica ± pyrophyllite ± sudoite + chlorite. These are replaced, at increasing tectonic depths, by a simpler muscovite ± chlorite assemblage, which also contains minor paragonite or margarite, in addition to muscovite. The estimated pressures during metamorphism showed a marked increase, as deduced from the *b* parameter of phengite. The Crestellina unit shows a low-pressure facies, according to the nomenclature of Guidotti and Sassi (1986), reaching the high-pressure facies in the Jubrique unit. The lower-temperature, dickite-bearing assemblage, characteristic of the upper units from the central zone of the Cordillera (Ruiz Cruz *et al.*, 2005), was not found in the Casares area.

From this preliminary study, three samples representative of the lithologies present in the several units, and showing different metamorphic grades, were selected for a detailed study (Table 1). In addition, chemical data for micas from other samples from each unit have also been used in chemical plots.

METHODOLOGY

The XRD patterns of bulk rocks and two grain-size fractions (2−20 μm and <2 μm) were obtained using a Siemens D-5000 diffractometer, with Cu$K\alpha$ radiation and graphite monochromator, operated at 40 kV and 40 mA (Málaga University). For the XRD study of the fine fractions, oriented samples, which were air dried, solvated with ethylene glycol, and heated at 550ºC, were prepared. Silicon was used as an internal standard for the exact determination of the basal spacings of the micas. The illite Kübler index (KI) was measured as the width of the 10 Å peak at half of the maximum peak height, expressed in º2θ (Kübler, 1968), following the recommendations of Kisch (1991). Our KI measurements (y) were transformed into CIS (crystallinity index standard)

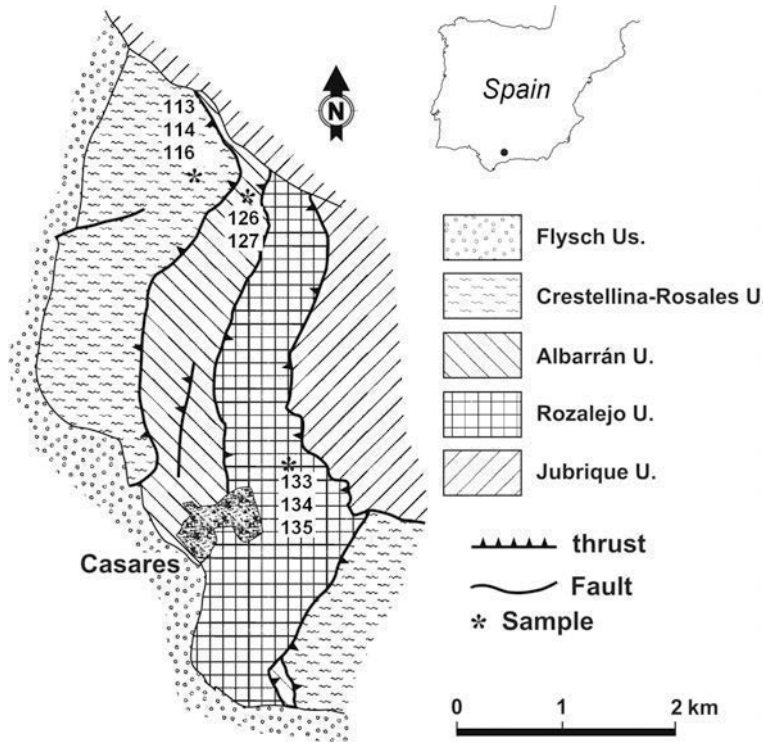

Figure 1. Schematic tectonic map of the Casares area and location of the samples studied (modified after Sanz de Galdeano *et al*., 1999).

values (x) (Warr and Rice, 1994) according to the equation $y = 1.23x - 0.07$. Decomposition of the mica peaks was carried out using the *Peakfit* software from Jandel Scientific. Peak fitting was performed using a Pearson IV function with the minimum number of components until correlation coefficients with r^2 >0.997 were achieved.

Polished and carbon-coated thin sections, selected on the basis of the XRD results, were imaged using back-scattered electrons and analyzed by SEM, using a Zeiss DSM 950 scanning electron microscope, equipped with an energy dispersive (EDX) system (Link QX 2000) at an accelerating voltage of 14 kV and beam current of 2 nA (CIC, Granada University). The beam size is on the

Table 1. Lithology and mineralogy of the selected samples.

Samples	Lithology	Mineralogy										
		Qtz	Ab	C	Cld	Ms	Na-K	Prg	Mrg	Chl	Sud	KI*
CL-113	Green sandstone	x				x	x	(x)		x	x	0.38–0.46
CL-126	Dark slate	x			(x)	x	x	(x)				0.32–0.43
CL-135	Blue phyllite	x	(x)	x		x		x	(x)	x		0.30–0.34
Additional samples used to obtain chemical data												
Crestellina unit												
CL-115	Red conglomerate	x	x			x	x			x	(x)	
CL-116	Red conglomerate	x	x			x	x	(x)				
Albarrán unit												
CL-127	Purple phyllite	x				x	x	x		x		
Rozalejo unit												
CL-133	White sandstone	x	(x)			x		(x)		x		
CL-134	Blue phyllite	x			x	x		x	(x)	x		

Mineral symbols according to Kretz (1983) except for C: calcite or dolomite, Na-K: intermediate Na-K white mica, and Sud: sudoite.
(x) Trace
KI*: Range of illite crystallinity indices in the tectonic slice.

order of 1 μm. The standards were albite (Na), orthoclase (K), periclase (Mg), wollastonite (Si and Ca), and synthetic oxides (Al_2O_3, Fe_2O_3, and $MnTiO_3$).

For the TEM/AEM study, washers were attached to selected areas and later separated from the glass backing. These areas were ion-thinned and carbon coated and examined in a 200 kV Jeol 2000 FX microscope, coupled with a Kevex Quantum X-ray energy-dispersive spectroscopic system (Universidad Complutense, Madrid), and in a 200 kV Philips CM-20 transmission electron microscope fitted with a scanning transmission device and solid state detector for energy-dispersive elemental analysis (EDX) (CIC, Universidad de Granada). The size of the areas analyzed ranged from 50 Å × 200 Å to 2000 Å × 2000 Å. Quantitative determinations used the thin-film approximation of Lorimer and Cliff (1976). Albite (Na), muscovite, and annite (K); albite, spessartine, and muscovite (Al); forsterite and annite (Mg and Fe); spessartine (Mn); and titanite (Ca and Ti) were used as standards. Lattice-fringe images were obtained using 00*l* reflections and underfocus conditions corresponding to maximum contrast. Chemical analyses were obtained for areas that were first characterized by electron diffraction and lattice-fringe imaging.

RESULTS

Although all units studied were submitted to a common Alpine metamorphic episode, the observed metamorphic variations are not only dependent on the depth of the units, but mainly on their paleogeographic position prior to the Alpine event, which varied from the typical Maláguide (extensional) to typical Alpujárride (collisional) settings (Ruiz Cruz *et al.*, 2006). The tectonic juxtaposition of these settings differentiates these sequences from those studied previously (*e.g.* Li *et al.*, 1992, 1994; Livi *et al.*, 1997), where the metamorphic evolution of the Na-bearing mica was observed in just one basinal setting.

Sample description

Sample CL-113 was taken in the upper tectonic unit (Crestellina). This sample is a green sandstone with poorly defined schistosity; it consists of quartz, quartzite, and large detrital mica grains (of the order of 0.1 mm). In addition, it contains a fine-grained matrix consisting of quartz, white mica, chlorite, and Fe oxide. The KI values measured in this unit range from 0.38 to 0.46, corresponding to the late diagenesis/low anchizone (Merriman and Peacor, 1999), although these values are influenced by the presence of Na-bearing micas. Micas from two conglomerates from this unit (Table 1), with dominant detrital mica, were also used for the chemical plots.

Sample CL-126, taken in the underlying Albarrán unit, is a dark slate, consisting mainly of fine-grained quartz and mica. Fe-, Ti-, and Fe+Ti-oxides are very abundant. Bedding is defined by Fe oxides (hematite) associated with elongated flakes of white mica (~100 μm long), whereas a well defined cleavage (S_1) is marked by dominant white mica. Small prisms of chloritoid parallel to S_1 were also identified. The KI values measured in associated Na-mica-free samples range from 0.32 to 0.43, which correspond to the low anchizone. Micas from a purple phyllite from this unit have also been used in the chemical plots.

Sample CL-135, belonging to the Rozalejo unit, is a phyllite with abundant dolomitic veins and textural characteristics similar to CL-126, although Fe oxides and Ti oxides are notably less abundant. The KI values determined in samples from this unit range from 0.30 to 0.34, corresponding to low–medium anchizone. In addition, micas from two other samples, a white sandstone and a blue phyllite with abundant chloritoid, were used in the chemical plots.

Previously published geochemical data (Ruiz Cruz *et al.*, 2006) revealed that, despite the variability of the SiO_2 contents, which are clearly dependent on the quartz content, the Al_2O_3 contents are large and homogeneous (~20%) in the selected samples.

XRD results

The mineralogical composition of the three samples, as deduced from the optical study and the XRD patterns, is shown in Table 1. Quartz, white mica, chlorite (Fe-rich chlorite in sample CL-113 and Mg-rich chlorite in sample CL-135), and minor albite are the main minerals identified in the XRD patterns of the bulk rocks. The <2 μm size fractions consist primarily of phyllosilicate assemblages (mica ± chlorite), with a small proportion of quartz. The XRD patterns of the <2 μm size fractions of the three samples display prominent splitting of the basal reflections of mica, indicating the presence of several micaceous phases. The presence of a relatively intense mica reflection at ~3.50 Å in the XRD patterns of the unoriented samples reveals that the micaceous phases are of $2M_1$ polytype. As a consequence, the XRD patterns of all micas were indexed on the basis of two-layer structure. We performed decompositions of the 002, 004, 006, and 00,10 reflections of micas. Although the fitting of the XRD data is not unique, the decompositions presented are those that provide the greatest correlation coefficients with a minimum number of components.

Decomposition of the ~10 Å peak from sample CL-113 (Figure 2a) permits the observation of three mica reflections at 10.02, 9.81, and 9.62 Å. In addition, a broad band at ~10.37 Å is also observed at the low-angle side of the 10 Å reflection, which probably corresponds to illite-rich illite-smectite mixed layers, although no change was observed after glycolation. Decomposition of the ~5 Å, ~3.3 Å, and ~2.0 Å mica peaks (Figure 2b,c,d) reveals, however, the presence of four

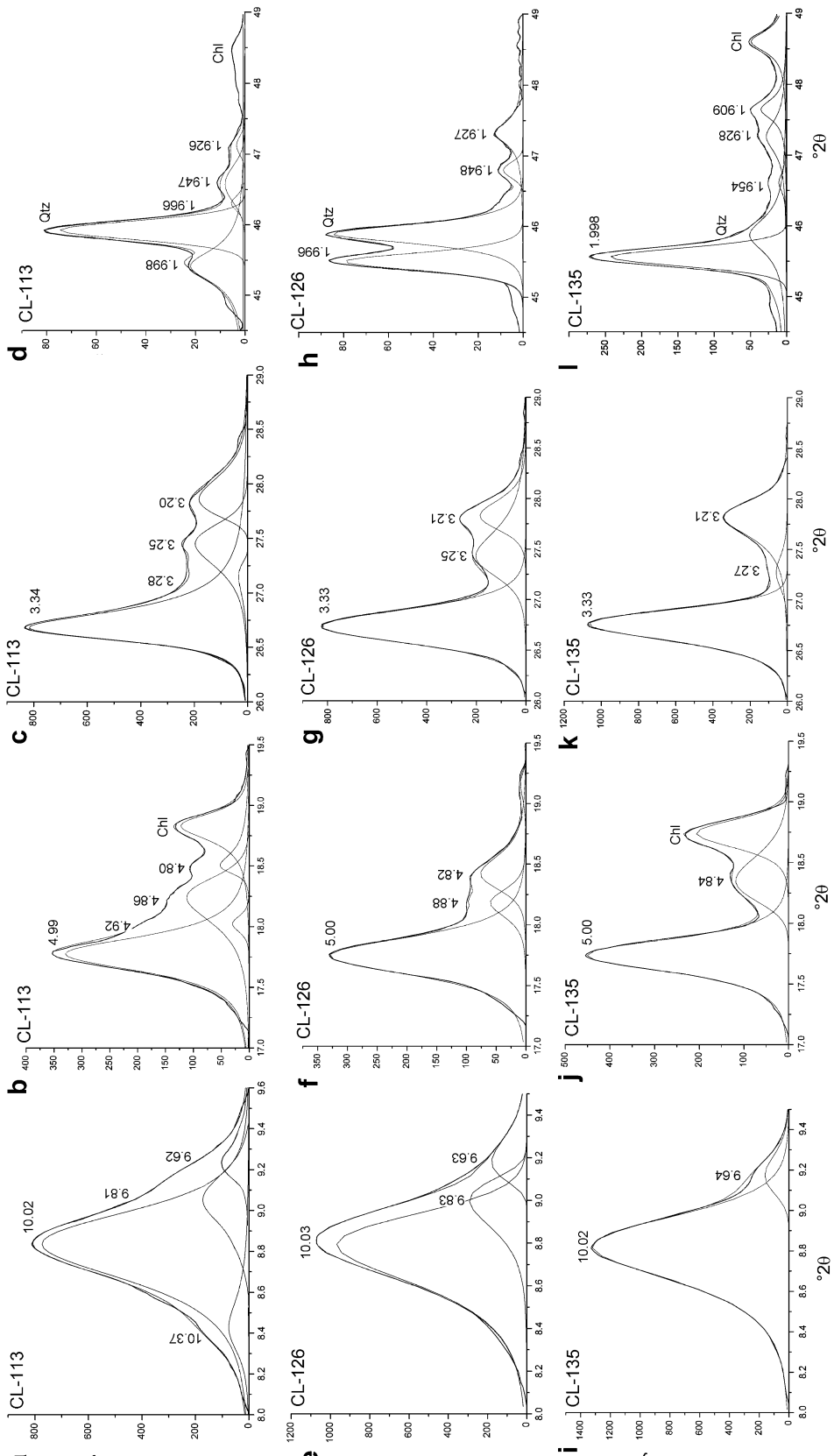

Figure 2. Selected zones of the XRD patterns of the <2 μm size fractions of the samples studied. (a, e, i) Positions of the 002 peaks of the micas. (b, f, j) Positions of the 004 reflections. (c, g, k) Positions of the 006 reflections. (d, h, l) Positions of the 00,10 reflections. Detailed explanation in the text.

mica reflections. The mean d_{001} of the four mica types and the approximate relative contents are: 19.98 Å (64%), 19.69 Å (5%), 19.47 Å (20%), and 19.26 Å (11%), which would correspond to muscovite (or illite), an intermediate phase with a muscovite:paragonite ratio of ~60:40, an intermediate phase with a muscovite:paragonite ratio of ~35:65, and paragonite. These latter values were calculated assuming a linear relation between Na content and position of the basal reflection, as demonstrated by Livi *et al.* (1997). Because the XRD patterns do not permit differentiation between solid solution and mixed layering (Jiang and Peacor, 1993; Li *et al.* 1994), the reflections of these intermediate phases could also correspond to mixed layers with Ms:Prg ratios of ~60:40 and ~35:65.

Decomposition of the ~10 Å, ~5 Å, ~3.3 Å, and ~2.0 Å peaks of white micas from sample CL-126 (Figure 2e–h) shows the presence of only three mica reflections. The mean d_{001} obtained for the three micas and the relative contents were: 19.96 Å (60%), 19.48 Å (20%), and 19.27 Å (20%), which correspond to muscovite, an intermediate phase with a muscovite:paragonite ratio of ~40:60, and paragonite, respectively.

Finally, decomposition of the three 002, 004, and 006 mica peaks from sample Cl-135 (Figure 2i–k) permits the observation of two mica reflections at 10.02–9.64 Å, 5.00–4.84 Å, and 3.33–3.21 Å. A weak band at ~3.27 Å was also observed after deconvolution of the 006 mica peaks, suggesting the presence of a minor amount of an intermediate phase. Decomposition of the 00,10 mica peaks (Figure 2l) reveals, in addition, the splitting of the reflection of the Na-bearing mica, indicating the contribution of a margarite-like mica. The mean d_{001} values and the relative contents obtained from the measured mica peaks were 19.98 Å (67%), 19.28 Å (16%), and 19.09 Å (17%).

In summary, the XRD results indicate the presence of two types of intermediate Na-K micas in the uppermost sample (CL-113), which coexist with minor paragonite. At increasing metamorphic grade (CL-126), a single intermediate Na-K mica is present. This assemblage is replaced by muscovite + paragonite + Ca-bearing mica in sample CL-135.

SEM study

Initial constraints on the composition of the white micas were obtained by SEM. Formulae of white micas were calculated on the basis of $O_{10}(OH)_2$ and assuming all Fe as Fe^{3+}, given the abundance of hematite in all the lithotypes studied. Representative formulae are shown in Table 2 and the most relevant chemical data have been plotted in Figure 3. White mica from samples of the Crestellina unit show very variable Si contents (3.00–3.46 a.p.f.u.), the largest values corresponding to large detrital grains such as that observed in Figure 4a. The Na content ranges between 0.06 and 0.40 a.p.f.u., and the interlayer occupancy between 0.66 and 0.96 a.p.f.u. The interlayer occupancies are especially small in detrital micas, including detrital biotite (not shown in the Table), probably due to weathering before sedimentation. Plots in Figure 3a–c reveal that the differences between detrital and authigenic mica are mainly reflected in the Si and the Na contents such that authigenic mica shows smaller Si contents and slightly larger Na contents, as seen in the average formulae (Table 2).

In samples from the Albarrán unit, bedding-parallel mica grains appear generally folded and contain abundant inclusions of Fe-, Ti-, and Fe+Ti-oxides. The largest, detrital grains show differences in contrast, correlating with the Na content (Figure 4b). The Na-enriched domains were not observed, however, in mica grains parallel to S_1, which show a uniform contrast (Figure 4c). The detrital population shows, in addition, a greater compositional variability than mica parallel to S_1. Plots in Figure 3d–f show that both bedding- and S_1-parallel micas display almost parallel trends. Moreover, both mica populations show more uniform average compositions, in contrast with the micas from the upper Crestellina unit.

Micas from the Rozalejo unit (Table 2, Figure 3g–i) show chemical trends similar to those observed in samples from the upper Albarrán unit, although differentiation among detrital and authigenic micas was not possible in this sample. The interlayer occupancy (~0.90 a.p.f.u.) is greater than in the other units, in accord with the higher metamorphic grade of this unit. The Ca content is generally small (<0.02 a.p.f.u.), although this content increases at the outermost areas of some grains; these areas show, in addition, smaller Si contents.

As a whole, micas from the three units do not show a positive correlation between Si and Fe+Mg. The lack of a clear phengitic trend is probably due to both the illitic substitution and the crystallochemical control of the Na contents on the Fe+Mg content (Guidotti and Sasssi, 1998), in such a way that the micas rich in both Si and Na have generally small Fe+Mg contents. Another common characteristic is the large Na contents in both detrital and authigenic micas, clearly within the miscibility gap characteristic of the low-temperature white mica (Chatterjee and Flux, 1986; Essene, 1989; Roux and Hovis, 1996). Since the XRD patterns indicate the presence of micas with different Na:K ratios, the grains studied by SEM must consist of intergrowths of several mica populations. Increasing metamorphic grade, characterizing the passage from Maláguide- to Alpujárride-like units, leads to greater mean interlayer occupancies and greater mean Si contents in the authigenic micas.

TEM/AEM study

The combined TEM/AEM observation of the fine-grained matrix of sample CL-113 reveals the presence of abundant grains of Na-rich muscovite and minor amounts of composite crystals containing muscovite,

Table 2. Chemical data obtained at the SEM scale.

Crestellina	Micas from the matrix								Detrital micas							
	1	2	3	4	5	6	7	Av. (σ)	8	9	10	11	12	13	14	Av. (σ)
Si	3.05	3.08	3.11	3.13	3.14	3.16	3.19	3.11 (0.07)	3.13	3.19	3.22	3.25	3.31	3.35	3.43	3.27 (0.09)
^{IV}Al	0.95	0.92	0.89	0.87	0.86	0.84	0.81	0.89 (0.07)	0.87	0.81	0.78	0.75	0.69	0.65	0.57	0.73 (0.09)
^{VI}Al	1.84	1.84	1.82	1.84	1.96	1.87	1.83	1.86 (0.07)	1.84	1.84	1.84	1.90	1.94	1.92	1.75	1.86 (0.05)
Ti	0.04	0.00	0.09	0.07	0.00	0.00	0.00	0.03 (0.03)	0.07	0.00	0.00	0.00	0.00	0.00	0.02	0.01 (0.03)
Fe	0.10	0.11	0.03	0.06	0.03	0.06	0.09	0.06 (0.05)	0.06	0.06	0.05	0.05	0.04	0.03	0.14	0.06 (0.03)
Mg	0.04	0.05	0.06	0.03	0.03	0.07	0.08	0.05 (0.03)	0.03	0.11	0.13	0.05	0.03	0.07	0.07	0.07 (0.05)
Σoct.	2.02	2.00	2.00	2.00	2.02	2.00	2.00	2.01 (0.06)	2.00	2.01	2.02	2.00	2.01	2.02	1.98	2.01 (0.03)
Ca	0.01	0.03	0.01	0.02	0.01	0.01	0.01	0.01 (0.01)	0.02	0.01	0.01	0.01	0.01	0.00	0.01	0.01 (0.01)
Na	0.27	0.30	0.07	0.27	0.39	0.06	0.22	0.23 (0.10)	0.27	0.06	0.06	0.07	0.30	0.07	0.21	0.15 (0.09)
K	0.54	0.61	0.76	0.46	0.41	0.80	0.60	0.59 (0.12)	0.46	0.78	0.76	0.74	0.37	0.60	0.44	0.59 (0.14)
Σint.	0.82	0.94	0.84	0.75	0.81	0.87	0.83	0.84 (0.06)	0.75	0.85	0.83	0.82	0.68	0.67	0.66	0.75 (0.07)

Albarrán	S_1-parallel micas								Bedding-parallel micas							
	1	2	3	4	5	6	7	Av. (σ)	8	9	10	11	12	13	14	Av. (σ)
Si	3.08	3.11	3.13	3.16	3.18	3.20	3.23	3.15 (0.04)	3.08	3.10	3.13	3.16	3.17	3.20	3.23	3.16 (0.06)
^{IV}Al	0.92	0.89	0.87	0.84	0.82	0.80	0.77	0.85 (0.04)	0.92	0.90	0.87	0.84	0.83	0.80	0.77	0.84 (0.06)
^{VI}Al	1.78	1.86	1.87	1.80	1.86	1.84	1.79	1.83 (0.05)	1.82	1.92	1.96	1.80	1.78	1.84	1.95	1.88 (0.11)
Ti	0.02	0.00	0.01	0.01	0.01	0.02	0.02	0.01 (0.02)	0.07	0.00	0.01	0.02	0.01	0.01	0.01	0.01 (0.03)
Fe	0.15	0.10	0.09	0.16	0.08	0.09	0.14	0.12 (0.05)	0.09	0.10	0.05	0.19	0.14	0.10	0.06	0.11 (0.07)
Mg	0.03	0.04	0.04	0.03	0.07	0.03	0.04	0.04 (0.03)	0.03	0.03	0.01	0.02	0.06	0.05	0.01	0.03 (0.03)
Σoct.	1.98	2.00	2.01	2.00	2.02	1.98	1.99	2.00 (0.03)	2.01	2.05	2.03	2.03	1.99	2.00	2.03	2.02 (0.02)
Ca	0.03	0.00	0.00	0.00	0.00	0.02	0.01	0.01 (0.01)	0.01	0.01	0.04	0.02	0.01	0.00	0.01	0.01 (0.01)
Na	0.29	0.12	0.18	0.31	0.16	0.20	0.22	0.21 (0.07)	0.22	0.36	0.49	0.38	0.32	0.14	0.08	0.29 (0.15)
K	0.64	0.78	0.67	0.55	0.64	0.62	0.56	0.63 (0.08)	0.65	0.3	0.22	0.32	0.56	0.75	0.56	0.47 (0.24)
Σint.	0.95	0.90	0.85	0.85	0.80	0.84	0.79	0.85 (0.08)	0.88	0.77	0.75	0.71	0.88	0.89	0.69	0.78 (0.09)

Rozalejo	1	2	3	4	5	6	7	8	9	10	11	12	13	14	15	Av. (σ)
Si	3.07	3.08	3.10	3.13	3.14	3.14	3.15	3.16	3.16	3.16	3.18	3.19	3.20	3.23	3.23	3.17 (0.04)
^{IV}Al	0.93	0.92	0.90	0.87	0.86	0.86	0.85	0.84	0.84	0.84	0.82	0.81	0.80	0.77	0.77	0.83 (0.04)
^{VI}Al	1.85	1.82	1.85	1.86	1.85	1.82	1.83	1.86	1.83	1.86	1.80	1.81	1.82	1.90	1.73	1.82 (0.08)
Ti	0.00	0.00	0.01	0.00	0.00	0.00	0.01	0.00	0.01	0.00	0.02	0.01	0.00	0.01	0.02	0.01 (0.01)
Fe	0.10	0.13	0.10	0.10	0.12	0.11	0.10	0.09	0.11	0.09	0.09	0.10	0.11	0.12	0.15	0.11 (0.04)
Mg	0.05	0.08	0.04	0.06	0.03	0.06	0.05	0.05	0.06	0.05	0.04	0.05	0.06	0.01	0.10	0.06 (0.03)
Σoct.	2.00	2.02	2.00	2.02	2.00	1.99	1.99	2.00	2.01	2.00	1.95	0.97	1.99	2.03	2.00	2.00 (0.03)
Ca	0.05	0.01	0.10	0.04	0.00	0.01	0.00	0.01	0.01	0.01	0.00	0.00	0.01	0.01	0.00	0.02 (0.03)
Na	0.26	0.17	0.20	0.21	0.15	0.16	0.13	0.15	0.13	0.15	0.06	0.13	0.16	0.41	0.08	0.17 (0.09)
K	0.63	0.76	0.62	0.61	0.77	0.78	0.79	0.76	0.75	0.76	0.81	0.76	0.74	0.27	0.77	0.70 (0.15)
Σint.	0.94	0.93	0.92	0.86	0.92	0.95	0.92	0.92	0.87	0.92	0.87	0.89	0.91	0.69	0.85	0.89 (0.05)

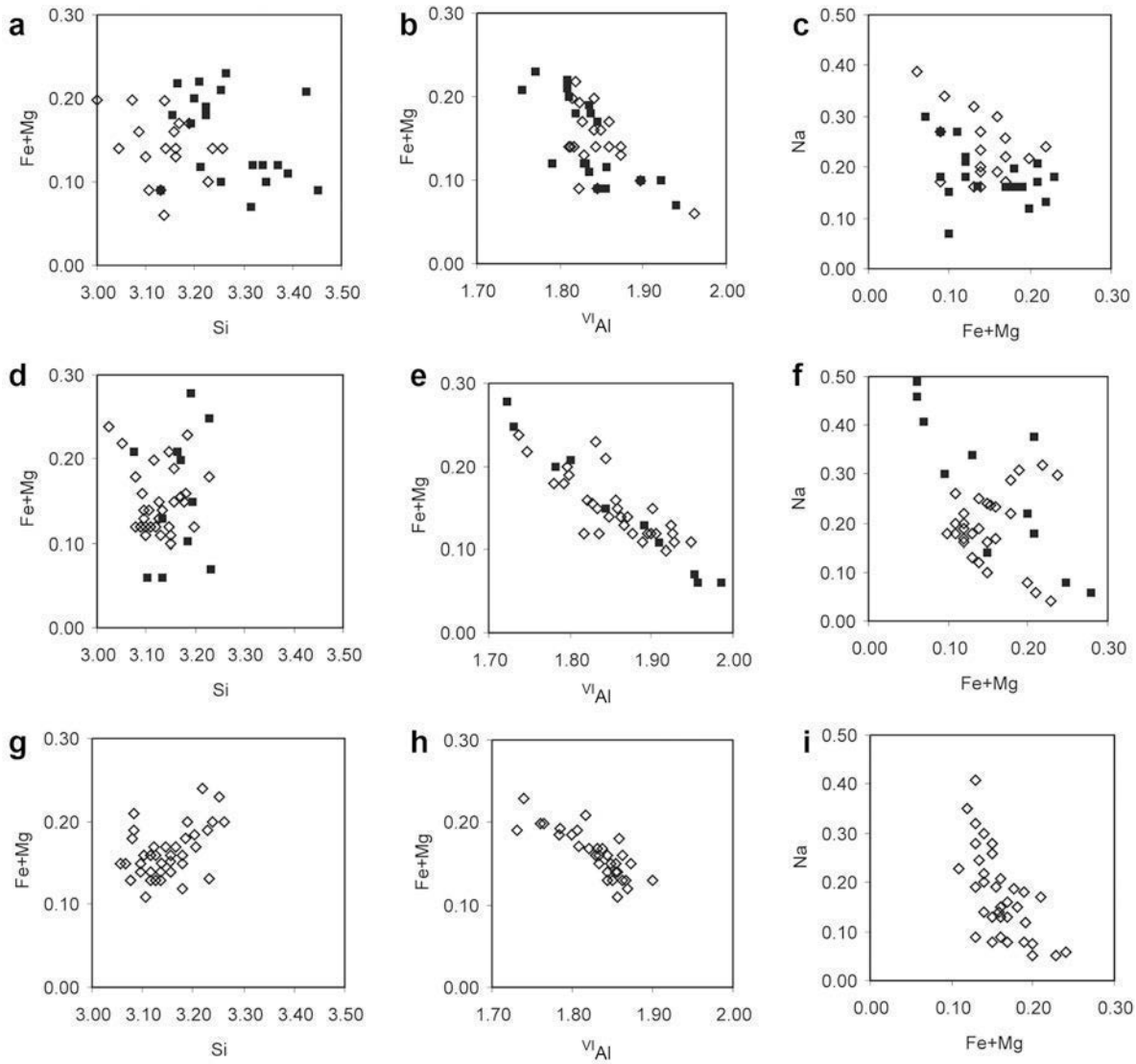

Figure 3. Chemical plots for samples of the three units studied. Data from the Crestellina unit (a–c) include, in addition to those obtained from sample CL-113, data from samples CL-115 and CL-116. The chemical data for the Albarrán (d–f) are from samples CL-126 and CL-127. The chemical data from the Rozalejo unit (G-I) were obtained from samples CL-133, CL-134, and CL-135. ◆: detrital grains in samples from Crestellina unit, and bedding-parallel micas (detrital in a part) in samples from Albarrán unit. ◇: authigenic grains.

paragonite (or brammallite), and packets with intermediate Na-K compositions (Figure 5a,b). The term 'grain' is used here for describing mica crystals large enough for observation at the SEM scale, and the term packet for a set of layers with apparent structural continuity and uniform chemical composition at the TEM scale. White micas commonly show low-angle boundaries, and the relative amount of Na-rich mica is variable from grain to grain. Most mica packets show sizes ranging from ~100 to ~500 Å in thickness (in some cases, as thin as 50 Å). Small differences in orientation between mica packets with different compositions permit the general identification of the 00*l* reflections of the several phases in the selected area electron diffraction (SAED) patterns (Figure 5b, inset). The lattice-fringe images of muscovite and paragonite (not shown) show a characteristic mottled aspect and lack of structural defects, and the SAED patterns correspond to well ordered two-layer polytypes. The lattice-fringe images of packets with intermediate composition are characterized, on the contrary, by the presence of dark fringes with a variety of periodicities, ranging from 40 to 100 Å (Figure 6). These structures, which are lacking in illite and paragonite packets, suggest some ordering in the distribution of Na- and K-bearing layers, as also assumed by Li *et al.* (1994).

Some representative AEM data for the white micas from sample CL-113 are shown in Table 3. The

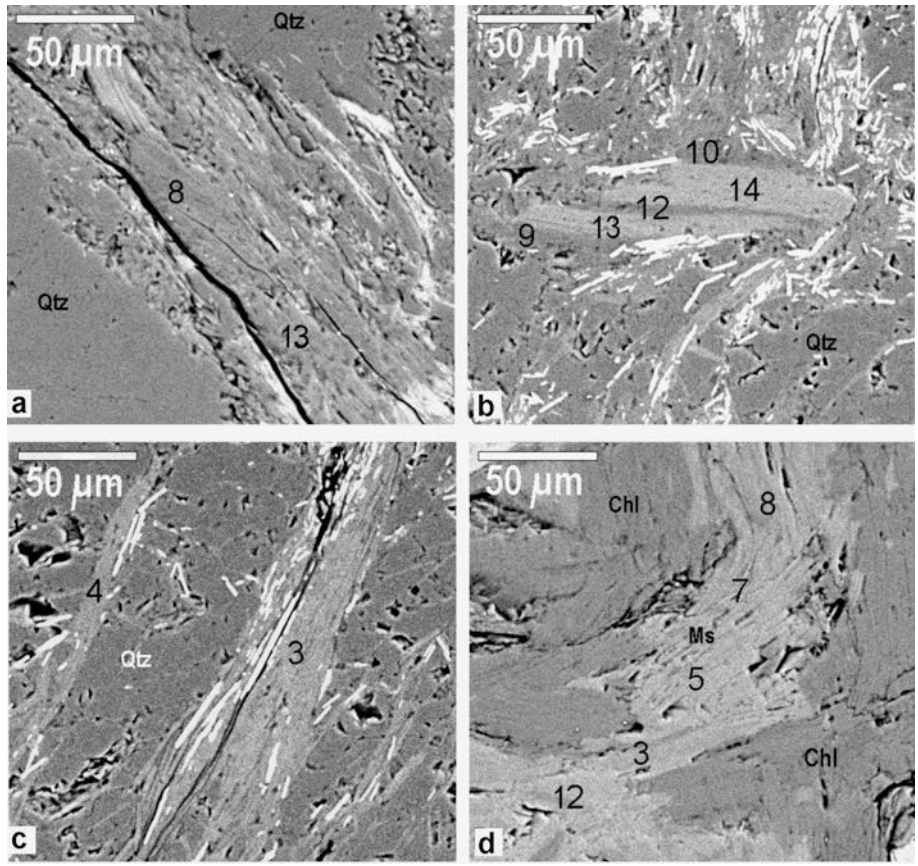

Figure 4. Backscattered electron microscopy images of mica grains. (a) Detrital mica grain from sample CL-113. Light areas are chlorite. (b) Detrital mica grain parallel to S_0 in sample CL-126. This grain is formed by parallel domains with variable contrast and Na contents. (c) Mica grains parallel to S_1 in sample CL-126. In parts b and c, prismatic light crystals are Fe-, Ti-, and Fe+Ti-oxides. (d) Intergrowths of white mica and Mg-rich chlorite from sample CL-135. The numbers correspond to analyses shown in Table 2. The mineral symbols are according to Kretz (1983) except for the micas with intermediate composition.

paragonite packets range in composition from $Prg_{78}Ms_{22}$ to $Prg_{92}Ms_8$, and the Fe+Mg contents are <0.05 a.p.f.u. A series of analyses of Na-rich intermediate packets are close to $Ms_{40}Prg_{60}$. On the contrary, the limit between muscovite and K-rich intermediate packets cannot be established because the analyses obtained range from $Ms_{94}Prg_6$ to $Ms_{54}Prg_{46}$ (Figure 7). The intermediate packets have Fe+Mg contents ranging from 0.03 to

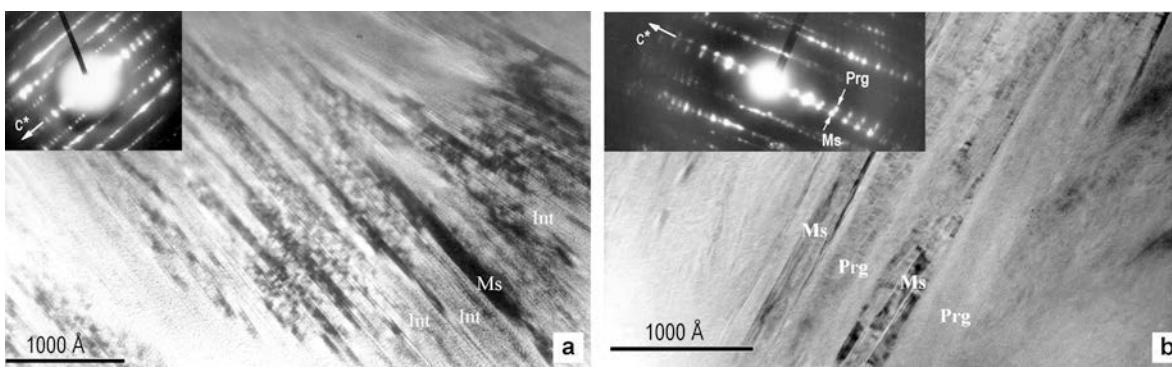

Figure 5. Low-magnification TEM images of white mica grains from sample CL-113. (a) Intergrowth of subparallel packets of muscovite and intermediate Na-K mica. The SAED pattern (inset) reveals the variable orientation of the *a** and *b** axes. (b) Parallel intergrowth of paragonite and muscovite. The reflections of the two phases can be observed in the SAED pattern (inset). Int: Intermediate Na-K mica.

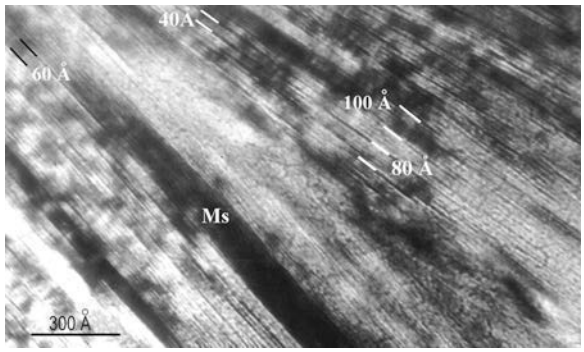

Figure 6. Lattice-fringe image of a mica packet with intermediate composition from sample CL-113. Dark fringes with high periodicities (from 40 to 100 Å) probably correspond to randomly ordered Prg-Ms mixed layers, with variable Ms:Prg ratios.

0.12 a.p.f.u. This content increases in typical muscovite analyses up to 0.25 a.p.f.u.

Sample CL-126 is characterized by the presence of parallel intergrowths of muscovite, paragonite, and packets with intermediate Na-K compositions, in variable combinations (Figure 8). Muscovite, paragonite, and Na-K intermediate packets commonly show a common orientation of the *c** axis and variable orientations of the *a** and *b** axes (Figure 8a,b inset). The coexistence of several mica types within a single mica grain is, in some cases, observed in the SAED patterns (Figure 8a). The mica packets are notably thicker than in the diagenetic sample, ranging between ~1000 and ~2000 Å. No significant textural differences were observed between bedding- and S_1-parallel mica grains. The lattice-fringe images of muscovite and paragonite are similar to those observed in sample CL-113. Packets with intermediate composition show, in some cases, wavy fringes (Figure 9). This textural characteristic could reflect structural distortions caused by the presence of K- or Na-rich domains (~100 Å) along the interlayer. The SAED patterns reflect, however, a two-layer ordered structure (Figure 9, inset).

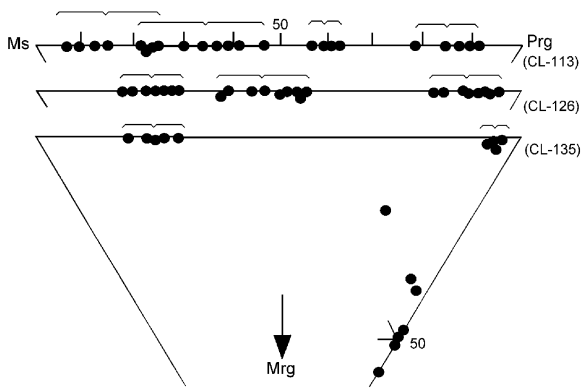

Figure 7. Plot of the AEM data for the three samples studied by TEM, on a ternary Ms-Prg-Mrg diagram.

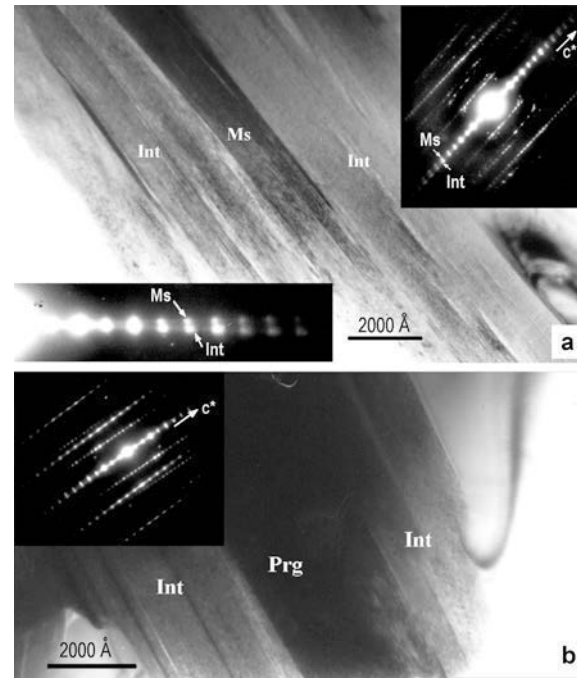

Figure 8. (a) Parallel intergrowth of Na-K intermediate mica and muscovite, from sample CL-126. The SAED pattern (inset) reveals that the lattices of the two micas only share the *c** axis. The enlarged image of the 00*l* reflection rows permits the observation of the muscovite and intermediate mica reflections. (b) Parallel intergrowth of paragonite and Na-K mica. The lattices of the micas also show variable orientations. Int: Intermediate Na-K mica.

Some representative analyses of the white micas from this sample are shown in Table 3. The variation in Na content can also be seen in Figure 7. Three populations of mica are observed in this sample: paragonite packets range in composition between $Prg_{94}Ms_6$ and $Prg_{82}Ms_{18}$. The composition of the muscovite grains ranges from $Ms_{87}Prg_{13}$ to $Ms_{70}Prg_{30}$. Finally, a third population of

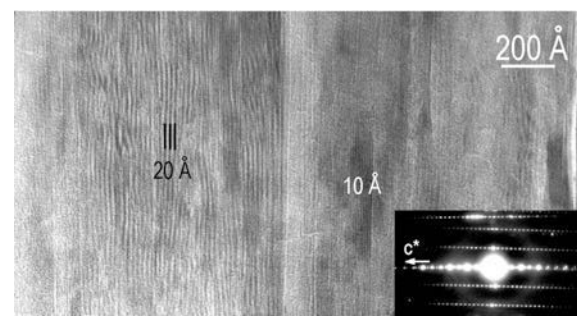

Figure 9. Lattice-fringe image of intermediate Na-K mica from sample CL-126. This packet shows areas with 10 Å and 20 Å periodicity, the latter with a characteristic wavy aspect. The SAED pattern (inset) indicates a two-layer polytype. Analysis 4 of this sample, shown in Table 3, corresponds to the left part of the image.

Table 3. Representative AEM data for white micas.

	CL-113						CL-126						CL-135				
	2 (Ms) Fig. 5a	7 (Ms) Fig. 5b	3 (Int) Fig. 5a	15 (Int) Fig. 5b	16 (Int) Fig. 6	9 (Prg) Fig. 5b	6 (Ms) Fig. 8a	11 (Ms) n.s.	2 (Int) Fig. 8a	4 (Int) Fig. 9	3 (Prg) Fig. 8b	9 (Prg) n.s.	10 (Ms) Fig. 10a	2(Ms) Fig. 10a	3 (Int) Fig.10a	5 (Int) Fig. 10b	9 (Prg) Fig. 10a
Si	3.25	3.12	3.12	3.20	3.07	3.11	2.99	3.09	3.16	3.13	3.36	3.09	3.12	3.18	2.50	2.52	2.91
^{IV}Al	0.75	0.88	0.86	0.70	0.93	0.89	1.01	0.91	0.84	0.87	0.64	0.91	0.88	0.82	1.50	1.48	1.09
^{VI}Al	1.79	1.83	1.98	1.89	2.03	2.00	1.92	1.88	1.97	2.00	1.94	2.02	1.85	1.78	1.99	2.02	1.99
Ti	0.00	0.00	0.00	0.00	0.00	0.00	0.00	0.00	0.00	0.00	0.00	0.00	0.00	0.02	0.00	0.00	0.00
Fe	0.10	0.14	0.07	0.06	0.03	0.04	0.09	0.07	0.04	0.00	0.00	0.02	0.13	0.15	0.05	0.04	0.04
Mg	0.15	0.08	0.00	0.06	0.00	0.00	0.08	0.09	0.00	0.00	0.00	0.00	0.08	0.10	0.00	0.00	0.06
Σoct.	2.04	2.05	2.05	2.01	2.06	2.04	2.08	2.04	2.01	2.00	1.94	2.04	2.06	2.05	2.04	2.08	2.09
Ca	0.01	0.00	0.01	0.00	0.00	0.00	0.01	0.00	0.01	0.02	0.02	0.02	0.00	0.00	0.50	0.43	0.02
Na	0.05	0.20	0.24	0.43	0.47	0.76	0.19	0.26	0.26	0.44	0.70	0.69	0.17	0.23	0.34	0.42	0.85
K	0.76	0.61	0.47	0.39	0.31	0.05	0.63	0.60	0.52	0.39	0.08	0.08	0.60	0.58	0.01	0.06	0.03
Σint.	0.82	0.81	0.72	0.82	0.78	0.82	0.83	0.86	0.79	0.85	0.80	0.79	0.77	0.81	0.85	0.91	0.90
Ca*	0.01	0.00	0.01	0.00	0.00	0.00	0.01	0.00	0.01	0.03	0.03	0.03	0.00	0.00	0.58	0.49	0.01
Na*	0.06	0.25	0.33	0.56	0.61	0.92	0.12	0.30	0.32	0.52	0.82	0.89	0.21	0.26	0.41	0.48	0.95
K*	0.93	0.75	0.66	0.44	0.39	0.08	0.87	0.70	0.68	0.45	0.15	0.08	0.79	0.74	0.01	0.03	0.04

Ms: muscovite; Prg: paragonite; Int: micas with intermediate Na-K or Na-Ca composition.n.s.: not shown in any of the figures
Ca*: Ca/(Ca+Na+K); Na*: Na/(Ca+Na+K); K*: K/(Ca+Na+K

packets ranging in composition between $Ms_{62}Prg_{38}$ and $Ms_{42}Prg_{58}$ corresponds to the intermediate Na-K-mica. Paragonite packets show very low Fe+Mg contents (<0.05 a.p.f.u.), whereas this content increases up to 0.17 a.p.f.u. in the muscovite packets.

Muscovite grains with high Na content dominate in sample CL-135. In addition, muscovite-paragonite intergrowths and more complex intergrowths with variable proportions of muscovite, paragonite, and intermediate Na-Ca mica are also frequent. Some of these composite grains (or stacks) also contain chlorite packets. In contrast to the other samples, micas with a Na-K intermediate composition were not identified in CL-135. A size increase of the mica packets, relative to sample CL-126, is observed, most packets being >2000 Å thick (Figure 10a). The SAED patterns reveal that all micas are two-layer polytypes. Low-magnification images show oblique and irregular boundaries between Ca-bearing packets and paragonite (Figure 10a), suggesting a secondary replacement of paragonite. Lattice-fringe images

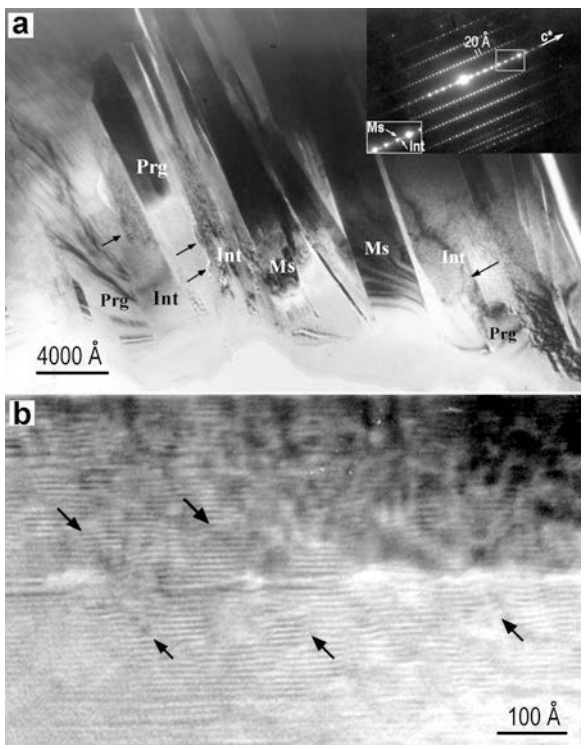

Figure 10. (a) Low-magnification TEM image of a stack consisting of paragonite, muscovite, and Na-Ca intermediate mica. The SAED pattern (inset) suggests that all micas are two-layer polytypes. Arrows mark the irregular boundaries between paragonite and packets with intermediate composition. Int: Intermediate Na-Ca mica. (b) Lattice-fringe image of a packet with Na-Ca intermediate composition. It shows wavy fringes with abundant structural defects. Arrows point to organization of fringes forming oblique angles with the basal planes. Numbers correspond to analyses of this sample shown in Table 3. Analysis 5 corresponds to part b.

of paragonite and muscovite show homogeneous 20 Å periodicity and lack of structural defects. In contrast, packets with Na-Ca- intermediate composition show wavy lattice fringes, with considerable changes in contrast over short distances. Some of these images also show that the contrast is organized along directions oblique to the basal plane (Figure 10b), as also observed by Livi *et al.* (1997) for intermediate Na-K-Ca micas. This feature was interpreted by those authors as due to segregation of immiscible cations into domains elongated along directions oblique to the basal planes.

Selected AEM analyses of the several white micas from this sample are shown in Table 3. The compositional intervals are also shown in Figure 7. The muscovite packets show Na contents ranging in composition from $Ms_{69}Prg_{31}$ to $Ms_{79}Prg_{21}$. The Fe+Mg content is of the order of 0.25 a.p.f.u. Paragonite shows a more restricted composition, close to $Prg_{95}Ms_2Mrg_3$. The packets with intermediate Na-Ca composition show some variability, but the average analysis is near to $Prg_{50}Mrg_{50}$. In contrast to muscovite, paragonite and Ca-bearing mica show Fe+Mg contents <0.10 a.p.f.u. In addition, packets with high Ca content are also characterized by high Al contents.

DISCUSSION

Chemical and structural changes of Na-bearing micas

Increasing metamorphic grade, at the passage from the upper tectonic slice (Crestellina) to the lowest one (Rozalejo), is reflected in clear changes of both composition and textural characteristics of the Na-bearing white micas. The XRD patterns show that the diagenetic sample contains four white-mica populations, including muscovite, paragonite, and intermediate Na-K mica with two main K:Na ratios, 60:40 and 35:45. Although the XRD patterns do not permit the unambiguous differentiation between solid solution and mixed-layering of paragonite and muscovite (Livi *et al.* 1997; Giorgetti *et al.* 2003), these ratios could correspond to randomly ordered sequences of muscovite and paragonite consisting of 3Ms+2Prg and 3Ms+4Prg, with main basal spacings ranging from ~50 to ~70 Å, as observed in TEM images (Figure 6). Some of these phases would be similar to the 6:4 mixed-layer paragonite-muscovite (or paragonite-phengite) described by Frey (1969, 1970), among others, in anchizonal to epizonal pelitic rocks, and probably represent structures with free-energy minima, kinetically favored at low temperature.

Anchizonal samples from the Albarrán unit show, in contrast, a single population of intermediate Na-K mica, as deduced from the XRD patterns. The mean composition corresponds to muscovite:paragonite ≈40:60. No evidence for ordering of K- and Na-layers was observed by TEM, suggesting that the packets with intermediate compositions consist of a solid solution of muscovite

and paragonite, as also observed by Jiang and Peacor (1993) and Giorgetti *et al.* (2003). Most packets with intermediate Na-K composition show lattice-fringe images with regular 10 or 20 Å periodicities, also suggesting a long-scale random distribution of Na and K in the structure. This strongly suggests that formation of an intermediate solid solution with composition ~$Prg_{60}Ms_{40}$ would be favored at anchizonal conditions, relative to the possible mixed-layered phases observed at diagenetic conditions. Nevertheless, the presence of nm-scale domains, which are occasionally suggested by TEM images (Figure 9), cannot be discarded on the basis of the available images.

In both the diagenetic sample from the Crestellina unit and the anchizonal sample from the Albarrán unit, mica grains are formed by lamellar intergrowths of parallel to subparallel packets of micas with interfaces parallel to the adjacent crystals (Figures 5–8). These textures are interpreted (see Jiang and Peacor, 1993) as formed through a dissolution-precipitation process because solid-state diffusion is sluggish and because the compositional changes require significant destruction and reconstruction of bonds.

Finally, Rozalejo samples simply contain discrete muscovite and paragonite, as deduced from the XRD patterns, whereas intermediate Na-K-micas are lacking. The TEM/AEM study reveals the presence of micas with composition intermediate between paragonite and margarite, coexisting with muscovite and paragonite. Packets of discrete margarite were not observed. At the SEM scale, Na-Ca intermediate micas show irregular interfaces with the adjacent paragonite packets (Figure 10). The lattice-fringe images of the Na-Ca intermediate micas strongly resemble those shown by Livi *et al.* (1997), and Livi and Veblen (2004) for intermediate Na-K micas, suggesting that Na and Ca are distributed within the packets as small domains, oblique to the basal planes. This domainal structure has also been observed, at the SEM scale, in epizonal Na-K-white micas from equivalent Triassic sequences of the Rif (unpublished data), and seems to represent an approach to the stability, at increasing metamorphic grade. The occurrence of inclined interfaces is consistent with both replacement of paragonite by Ca-bearing mica and diffusion of the large alkali ions along layers.

In accordance with the XRD data, packets of intermediate Na-K micas show a wide range of Na/K ratio (see Figure 7) in sample CL-113. The passage from the diagenetic zone to the low anchizone (sample CL-126) causes an increase in the size of the mica packets, at the same time that the compositional range of the intermediate micas becomes narrower, as indicated by the AEM data (Figure 7).

The compositional changes of the Na-K-bearing micas are accompanied by changes in the composition of the coexisting K-rich mica and paragonite. Illite present in the diagenetic sample is replaced, at increasing metamorphic grade, by muscovite with high Na contents. The composition of paragonite follows, in appearance, an inverse trend with decreasing K content at increasing metamorphic grade.

A similar mineralogical evolution was described by Livi *et al.* (1997) at the diagenesis-anchizone transition in Liassic shales of Central Switzerland. Nevertheless, differences in detrital mineral assemblages between the Liassic shales from the Alps and the Triassic rocks described here suggest that the mechanisms of formation of the Na-bearing micas must be different, as discussed below.

Origin of Na-bearing micas

Smectite has commonly been considered as the most probable precursor phase for Na-K intermediate micas (*e.g.* Frey, 1969, 1970; Merriman and Roberts, 1985; Shau *et al.*, 1991; Li *et al.*, 1994). However, smectite is rare in Triassic shales from the diagenetic zone in Maláguide-like lithologies. R4 mixed-layer illite-smectite has been reported only occasionally in diagenetic samples (Abad *et al.*, 2003; this study). The lack of smectite in these units can be related to both the arid Triassic climate, which would prevent smectite formation in the source areas, and the continental depositional environment. We assume that the detrital components of Triassic Maláguide sequences consisted mainly of micas and minor chlorite. The early diagenetic processes produced the intensive dissolution of feldspar and, to a lesser extent, of mica, which was clearly favored in coarse-grained rocks. Concomitant with the dissolution was the formation of abundant kaolinite, which filled the pores in coarse-grained rocks and partially replaced muscovite. We also assume that a kaolinite to dickite transformation occurred during the Alpine metamorphic event at late diagenetic conditions (Ruiz Cruz and Andreo, 1996). Thus, the typical mineral assemblage of Triassic Maláguide rocks consists of illite+dickite. On the other hand, in coarse-grained Maláguide-type rocks, dickite was subsequently replaced by illite and chlorite. The white mica formed from dickite was Na free at diagenetic conditions whereas, at the transition from diagenesis to low anchizone, white mica incorporates large amounts of Na, leading to intermediate compositions similar to those found here in the late-diagenetic sample (unpublished results). Thus, although some detrital mica grains are Na-rich, dickite is the more probable precursor of authigenic Na-bearing white mica in the uppermost Maláguide-like sandstone. Although destabilization of detrital Na-bearing mica during the diagenetic processes might have provided Na for incorporation into authigenic mica, there are other possible Na sources, *e.g.* albite, which is a common detrital phase in these rocks.

To draw conclusions on the mineral evolution in Alpujárride-type rocks is difficult, because the higher metamorphic grade has obliterated the detrital assemblage to a large extent. The most common mineral assemblage, consisting of phengite+chlorite suggests that mica and

chlorite also were the main detrital components. The lack of dickite and pyrophyllite in Maláguide-like shales and in all Alpujárride-type rocks suggests, moreover, that the early diagenetic reactions were different from those observed in coarse-grained Maláguide rocks, probably due to their more distal deposition.

The presence of microscopic Na- and K-rich parallel domains in the large detrital grains from sample CL-126 (Figure 3b) suggests that intergrowths of Na- and K-micas were already present in the detrital assemblage, as observed in the overlying samples. Nevertheless, textural data indicate that the formation of Na-bearing micas also occurred during the diagenetic-to-metamorphic process, either from fine-grained detrital Na-bearing micas or from smectite or mixed-layer illite-smectite.

In addition, later recrystallization of mica during the prograde process does not lead to discrete packets of muscovite and paragonite only, as observed by Li *et al.* (1994). On the contrary, S_1-parallel mica grains from sample CL-126 also contain packets of mica with intermediate compositions, indicating that metastable, intermediate Na-K micas also grew during the dissolution-precipitation process that led to the S_1 mica formation. This strongly suggests that an intermediate mica with composition ~$Prg_{60}Ms_{40}$ represents a structure with a metastable free-energy minimum, kinetically favored at low temperature.

The formation of intermediate Na-Ca mica probably followed a different path. Ca-bearing mica has only been detected in the calcite-bearing sample (CL-135). In addition, SEM data indicate Ca enrichment in the outermost parts of the mica grains and the TEM images suggest a prograde replacement of paragonite by these intermediate micas. These data suggest that the formation of Ca-bearing micas occurred from paragonite, with calcite as the more probable source of Ca, as also assumed by Livi *et al.* (1997).

The fact that the mechanisms of formation of Na-bearing micas change in a relatively small temperature range (from late diagenesis to medium anchizone) suggests that these changes were controlled by other factors, in addition to temperature. The precursor phases were different in the various lithotypes, and the several structures do not necessarily represent sequential steps of a reaction progress as those described previously (*e.g.* Livi *et al.*, 1997). In addition, the change of geotectonic setting from low-pressure, in the upper slices, to high-pressure conditions, in the deeper ones, is another factor probably influencing the mechanisms of paragonite formation. Indeed, high-pressure conditions appear to favor the formation of paragonite (Guidotti, 1984).

CONCLUSIONS

This study describes the occurrence of white micas with variable intermediate compositions between muscovite and paragonite and between paragonite and margarite in Triassic rocks of the transition Maláguide-to-Alpujárride complexes. Both types of intermediate micas coexist with muscovite and paragonite.

Although some detrital grains contain Na-rich mica, incorporation of Na in the structure of the authigenic mica occurred mainly during the diagenetic-to-metamorphic process, the precursor phases probably being dickite, in the uppermost, coarse-grained rock, and mixed-layer illite-smectite or detrital illite, in the underlying, fine-grained samples. In appearance, the different precursor phases, and probably the change from extensional to collisional settings, notably influenced the mechanisms of formation, which would have changed from random mixed-layered structures in the diagenetic sample, to homogeneous solid solution of muscovite and paragonite, and then to a domainal structure in the Na+Ca-micas present in the more metamorphic sample.

ACKNOWLEDGMENTS

The author is grateful to two anonymous referees, whose suggestions improved the manuscript. The assistance of M.M. Abad (Universidad de Granada), and of J.L. Baldonedo and A. Gómez (Universidad Complutense) in obtaining TEM/AEM data is acknowledged. This study received financial support from the Project CGL 2006-02481 (Ministerio de Educación y Ciencia) and from the Research Group RNM-199.

REFERENCES

Abad, I., Nieto, F., Peacor, D.R., and Velilla, N. (2003) Prograde and retrograde diagenetic and metamorphic evolution in metapelitic rocks of Sierra Espuña (Spain). *Clay Minerals*, **38**, 1–23.

Ahn, J.H., Peacor, D.R., and Essene, E.J. (1985) Coexisting paragonite-phengite in blueschist eclogite: A TEM study. *American Mineralogist*, **70**, 1193–1204.

Azañón, J.M., Crespo-Blanc, A., and García-Dueñas, V. (1997) Continental collision, crustal thinning and nappe forming during the pre-Miocene evolution of the Alpujarride Complex (Alboran Domain, Betics). *Journal of Structural Geology*, **19**, 1055–1071.

Azañón, J.M., García-Dueñas, V., and Goffé, B. (1998) Exhumation of high-pressure metapelites and coeval crustal extension in the Alpujárride complex. *Tectonophysics*, **285**, 231–252.

Booth-Rea, G., Azañón, J.M., Goffé, B., Vidal, O., and Martínez-Martínez, J.M. (2002) High-pressure, low-temperature metamorphism in Alpujarride Units of southeastern Betics (Spain). *Comptes Rendues Académie Sciciences Série Geosciences*, **334–11**, 857–865.

Boundy, T.M., Hall, C.M., Li, G., Essene, E.J., and Halliday, A.N. (1997) Fine-scale isotopic heterogeneities and fluids in the deep crust: a $^{40}Ar/^{39}Ar$ laser ablation and TEM study of muscovites from a granulite-eclogite transition zone. *Earth and Planetary Science Letters*, **148**, 223–242.

Chatterjee, N.D. and Flux, S. (1986) Thermodynamic mixing properties of muscovite-paragonite crystalline solutions at high temperatures and pressures, and their geological applications. *Journal of Petrology*, **27**, 677–693.

Essene, E.J. (1989) The current status of thermobarometry in metamorphic rocks. Pp. 1–44 in: *Evolution of Metamorphic Belts* (J.S. Daly and B.W.D. Yardley, editors). Special Publications, **43**, Geological Society, London.

Ferrow, E.A., London, D., Goodman, K.S., and Veblen, D.R. (1990) Sheet silicates of the Lawler Peak granite, Arizona: chemistry, structural variations and exsolution. *Contributions to Mineralogy and Petrology*, **105**, 491–501.

Frey, M. (1969) A mixed-layer paragonite/phengite of low-grade metamorphic origin. *Contributions to Mineralogy and Petrology*, **24**, 63–65.

Frey, M. (1970) The steps from diagenesis to metamorphism in pelitic rocks during Alpine orogenesis. *Sedimentology*, **15**, 261–279.

Frey, M. (1987) Very low-grade metamorphism of clastic sedimentary rocks. Pp. 9–58 in *Low-temperature Metamorphism* (M. Frey, editor). Blackie, Glasgow, UK.

Giorgetti, G., Monecke, T., Kleeberg, R., and Herzig, P.M. (2003) Intermediate sodium-potassium mica in hydrothermally altered rocks of the Waterloo deposit, Australia: a combined SEM-EMP-SRD-TEM study. *Contributions to Mineralogy and Petrology*, **146**, 159–173.

Goffé, B., Michard, A., García-Dueñas, V., González-Lodeiro, F., Monié, P., Campos, J., Galindo-Zaldívar, J., Jabaloy, A., Martínez-Martínez, J.M., and Simancas, F. (1989) First evidence of high-pressure, low temperature metamorphism in the Alpujarride nappes, Betic Cordillera (SE Spain). *European Journal of Mineralogy*, **1**, 139–142.

Guidotti, C.V. (1984) Micas in metamorphic rocks. Pp. 357–467 in: *Micas* (S.W. Bailey, editor). Reviews in Mineralogy, **13**, Mineralogical Society of America, Washington, D.C.

Guidotti, C.V. and Sassi, F.P. (1986) Classification and correlation of metamorphic facies series by means of muscovite b_o data from low grade metapelites. *Neues Jahrbuch für Mineralogie Abhandlungen*, **153**, 363–380.

Guidotti, C.V. and Sassi, F.P. (1998) Petrogenetic significance of Na-K white mica mineralogy: Recent advances for metamorphic rocks. *European Journal of Mineralogy*, **19**, 815–854.

Jiang, W.-T. and Peacor, D.R. (1993) Formation and modification of metastable sodium potassium mica, paragonite and muscovite in hydrothermally altered metabasites from northern Wales. *American Mineralogist*, **78**, 782–793.

Kisch, H.J. (1983) Mineralogy and petrology of burial diagenesis (burial metamorphism) and incipient metamorphism in clastic rocks. Pp. 289–493 in: *Diagenesis in Sediments and Sedimentary Rocks* (G. Larsen and G.V. Chilingar, editors). Elsevier, New York.

Kisch, H.J. (1991) Illite crystallinity; recommendations on sample preparation, X-ray diffraction settings, and interlaboratoy samples. *Journal of Metamorphic Geology*, **9**, 665–670.

Kretz, R. (1983) Symbols for rock-forming minerals. *American Mineralogist*, **68**, 277–279.

Kübler, B. (1968) Evaluation quantitative du métamorphisme par la cristallinité de l'illite. Etat des progrès réalisés ces dernières années. *Bulletin de Centre Recherches Pau, S.N.P.A.*, **2**, 385–397.

Li, G., Jiang, W.-T., and Peacor, D.R. (1992) Metastable intermediate Na/K micas in hydrothermally altered metabasites and metamorphosed pelites from Wales. *Geological Society of America, Abstract with Programs*, **31**, A72.

Li, G., Peacor, D.R., Merriman, R.J., and Roberts, B. (1994) The diagenetic to low-grade metamorphic evolution of matrix white micas in the system muscovite-paragonite in a mudrock from central Wales, United Kingdom. *Clays and Clay Minerals*, **42**, 369–381.

Livi, K.J.T. and Veblen, D.R. (2004) Long-range interlayer cation segregation during low-grade metamorphism of mica. 32nd IGC, Florencia. *Abstracts*, **1**, 307.

Livi, K.J.T., Veblen, D.R., Ferry, J.M., and Frey, M. (1997) Evolution of 2:1 layered silicates in low-grade metamorphosed Liassic shales of Central Switzerland. *Journal of Metamorphic Geology*, **15**, 323–344.

Lorimer, G.W. and Cliff, G. (1976) Analytical electron microscopy of minerals. Pp. 506–519 in: *Electron Microscopy in Mineralogy* (H.R. Wenk, editor). Springer-Verlag, New York.

Mäkel, G.H. (1985) The geology of the Maláguide complex and its bearing on the geodynamic evolution of the Betic-Rif orogen (Southern Spain and Northern Morocco). *Gua Papers Geology*, **22**, 263 pp.

Martín-García, J.M., Delgado, G., Sanchez Marañón, M., Parraga, J.F., and Delgado, R. (1997) Nature of dioctahedral micas in Spanish red soils. *Clay Minerals*, **32**, 107–121.

Merriman, R.J. and Roberts, B. (1985) A survey of white mica crystallinity and polytypes in pelitic rocks of Snowdonia and Llŷn, North Wales. *Mineralogical Magazine*, **49**, 305–319.

Merriman, R.J. and Peacor, D.R. (1999) Very low-grade metapelites: mineralogy, microfabrics and measuring reaction progress. Pp. 10–60 in: *Low-grade Metamorphism* (M. Frey and D. Robinson, editors). Blackwell Science, Oxford, UK.

Roux, J. and Hovis, G.L. (1996) Thermodynamic mixing models for muscovite-paragonite solutions based on solution calorimetric and phase equilibrium data. *Journal of Petrology*, **37**, 1241–1254.

Ruiz Cruz, M.D. and Andreo, B. (1996) Genesis and transformation of dickite in Permo-Triassic sediments (Betic Cordilleras, Spain). *Clay Minerals*, **31**, 133–152.

Ruiz Cruz, M.D. and Rodríguez Jiménez, P. (2002) Correlation between crystallochemical parameters of phyllosilicates and mineral facies in very low-grade metasediments of the Betic Cordillera (Spain): A synthesis. *Clay Minerals*, **37**, 169–185.

Ruiz Cruz, M.D., Sanz de Galdeano, C., and Lázaro, C. (2005) Metamorphic evolution of Triassic rocks from the transition zone between the Maláguide and the Alpujárride complexes (Betic Cordilleras, Spain). *European Journal of Mineralogy*, **17**, 81–91.

Ruiz Cruz, M.D., Franco, F., Sanz de Galdeano, C., and Novak, J. (2006) Evidence of contrasting low-grade metamorphic conditions from clay mineral assemblages in Triassic Alpujárride-Maláguide transitional units in the Betic Cordilleras, Spain. *Clay Minerals*, **41**, 619–636.

Sanz de Galdeano, C., López Garrido, A.C., and Andreo, B. (1999) The stratigraphic and tectonic relationhips of the Alpujárride and Maláguide complexes in the western Betic Cordillera (Casares, Prov. of Malaga, South Spain). *Comptes Rendus Académie Sciences, Paris*, **328**, 113–119.

Sanz de Galdeano, C., Andreo, B., García-Tortosa, F.J., and López-Garrido, A.C. (2001) The Triassic palaeogeographic transition between the Alpujárride and Maláguide complexes. Betic-Rif Internal Zone. *Palaeo*, **167**, 157–173.

Shau, Y.-T., Feather, M.E., Essene, E.J., and Peacor, D.R. (1991) Genesis and solvus relations of submicroscopically intergrown paragonite and phengite in a blueschist from northern California. *Contributions to Mineralogy and Petrology*, **106**, 367–378.

Warr, L.C. and Rice, H.N. (1994) Interlaboratory standardization and calibration of clay minerals crystallinity and crystallite size data. *Journal of Metamorphic Geology*, **12**, 141–152.

(*Received 16 October 2007; revised 10 March 2008; Ms. 0091; A.E. D. McCarty*)